Nanotechnology **11** (2000) 173–180. Printed in the UK PII: S0957-4484(00)09682-3

Molecular dynamics simulation of phase transformations in silicon monocrystals due to nano-indentation

W C D Cheong and L C Zhang†

Department of Mechanical and Mechatronic Engineering, The University of Sydney, NSW 2006, Australia

Received 18 November 1999, in final form 6 June 2000

Abstract. This paper discusses the phase transformation of diamond cubic silicon under nano-indentation with the aid of molecular dynamics analysis using the Tersoff potential. By monitoring the positions of atoms within the model, the microstructural changes as silicon transforms from its diamond cubic structure to other phases were identified. The simulation showed that diamond cubic silicon transforms into a body-centred tetragonal form (β-silicon) upon loading of the indentor. The change of structure is accomplished by the flattening of the tetrahedron structure in diamond cubic silicon. Upon unloading, the body-centred tetragonal form transforms into an amorphous phase accompanied by the loss of long-range order of the silicon atoms. By performing a second indentation on the amorphous zone, it was found that the body-centred-tetragonal-to-amorphous phase transformation could be a reversible process.

(Some figures in this article are in colour only in the electronic version; see `www.iop.org`)

1. Introduction

The phase transformation of diamond cubic silicon due to indentation has been the subject of much literature. According to these studies, the initial plastic deformation during indentation is accompanied by a densifying semiconductor-to-ductile-metal phase transformation. Upon unloading, a tetragonal-body-centred-to-amorphous-semiconductor phase transformation is observed [1]. The conclusions are supported by several studies carried out using electrical resistance [2–7], x-ray diffraction [8–12] and optical properties [13–15]. These experimental studies revealed that silicon transformed from its diamond cubic structure to a metallic body-centred tetragonal structure, known also as β-silicon. In the experiments, the metallic nature of the β-silicon phase is inferred by the fall in the resistivity of silicon by a few orders of magnitude during indentation. Diffraction patterns obtained during indentation also lend credence to the transformation of silicon from its diamond cubic to the body-centred tetragonal phase. Although these experiments have furnished us with a wealth of information, combining the information into a convincing picture of the microscopic mechanisms of the phase transition is impeded by possible ambiguities in interpreting these experimental findings. Ideally one would want to directly observe the atomic-scale processes involved in the phase transformation. Such an experiment can be more easily carried out with computer simulations, in particular using the molecular dynamics method. In this present study, molecular dynamics is used to simulate the effects of nano-indentation on a silicon monocrystal. This method allows for the simulation of the phase transition without any assumption on the nature of the phases. The atoms are placed on perfect positions at the beginning, and the resulting structures only depend on the thermo-mechanical conditions and the interaction forces between atoms, as defined by the potential function. The simulation reveals that silicon transforms from its diamond cubic structure into a body-centred tetragonal form in the region directly beneath the indentor during indentation and transforms into an amorphous phase upon unloading of the indentor. The structure of the tetragonal form obtained is similar to that of β-silicon. Hence, though molecular dynamics does not reproduce the real experiments due to differences in time and size scale, the simulation provides possible theoretical evidence of the phase transformation observed in the experiments quoted above and enables us to better understand the mechanisms involved in such a transformation. As a first step in this direction, it is necessary to establish the validity of the interatomic potential to be used in the atomistic simulations. The primary concern was to validate the ability of the chosen interatomic potentials to predict the stability of the various crystal structures involved. The potential functions used in the simulation and the molecular dynamics model will be discussed in the following section.

† Author for correspondence.

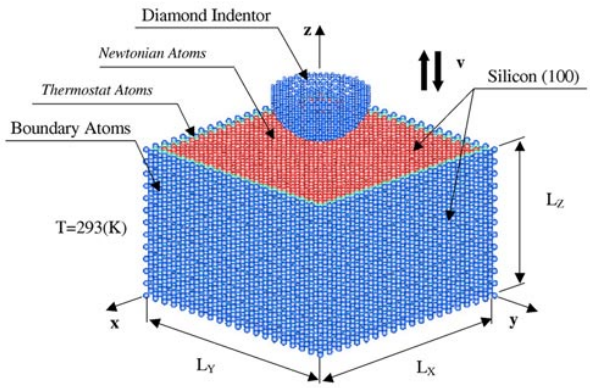

Figure 1. Molecular dynamics simulation model of silicon monocrystal and diamond indentor. The size of the control volume is $L_X \times L_Y \times L_Z$. In all the calculations, the velocity of the indentor $v = 40$ m s^{-1}.

2. Computation and modelling

2.1. Initial model

Figure 1 shows the model of a specimen of silicon monocrystal and diamond indentor used in the simulation. The hemispherical diamond indentor has a radius of 2.14 nm. The dimension of the control volume of the silicon specimen has to be made sufficiently large to eliminate boundary effects. Taking this into consideration, an optimum control volume is chosen based on an iterative process of increasing the control volume size until further increases do not affect the displacement and velocities of the atoms due to the indentation process. An optimum size of $6.5 \times 10.3 \times 10.3$ nm^3 is obtained for this simulation. Figure 2 shows the displacement field of the atoms at the maximum indentation for the optimum control volume size, where the direction of an arrow indicates the direction of an atom displacement and the length of the arrow is the magnitude of displacement. It can be seen that the atoms affected by the indentor are primarily those near the indentor. Atoms away from that region do not displace from their equilibrium positions. To restrict the rigid-body motion of the specimen, layers of boundary atoms that are fixed in space are used to contain the Newtonian atoms with the exception of the top (100) surface, that is exposed to the indentor. Thermostat atoms are also used to ensure a reasonable outward heat conduction away from the control volume. The workpiece is made up of 36 341 atoms and the tool is made up of 1818 atoms.

2.2. Interatomic potentials

Before carrying out the molecular dynamics simulation on the indentation of silicon, it is important to ensure that the chosen potential function used gives a reliable result for the simulation. For covalent systems such as silicon, the directionality of bonding is important. Tersoff [16] proposed a simple pair-like potential where the bond order of the atoms is affected by its local environment. This replaces the two- and three-body potential conventionally employed when directionality of bonding is a concern. Based on empirical data, Tersoff [17] also verified that the Tersoff potential is capable of predicting stable phases of diamond cubic silicon

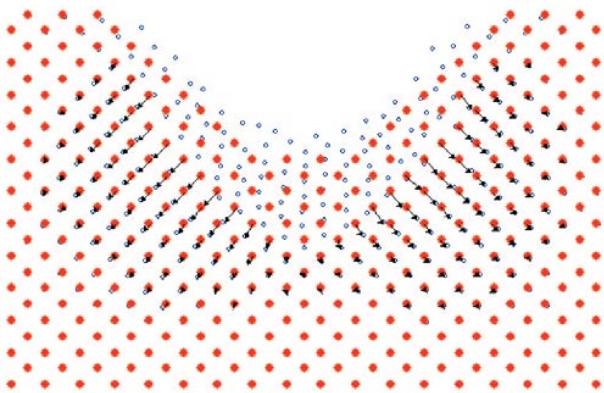

Figure 2. Displacement field of the atoms at the maximum indentation. The arrows represent the displacement of the atoms from their initial position before indentation to their new positions at the maximum indentation. The filled circles represent the equilibrium positions of the atoms while the smaller hollow circles represent the displaced positions of the atoms at maximum indentation.

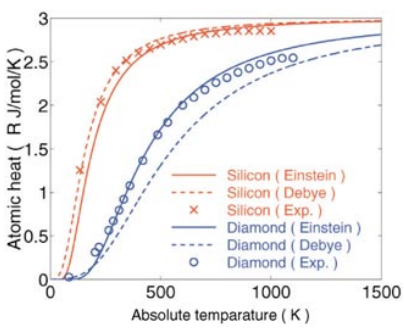

Figure 3. A comparison of the theoretical calculation of atomic heat with experimental measurement.

and body-centred tetragonal β-silicon. Hence the Tersoff potential is used in the present simulation to dictate the interaction between the silicon atoms. When assuming j and k are the neighbouring atoms of atom i, the atomic bond lengths of atoms i–j and i–k are r_{ij} and r_{ik} and the angle between bonds i–j and i–k is θ_{ijk}, then the total Tersoff energy E can be expressed as

$$E = \sum_i E_i = \tfrac{1}{2} \sum_{i \neq j} W_{ij}, \tag{1}$$

where W_{ij} is the bond energy, so the summation in the equation is over all the atomic bonds in the control volume. W_{ij} is a function of the repulsive pair potential f_{R} and the attractive pair potential f_{A}, and has the form

$$W_{ij} = f_{\mathrm{C}}(r_{ij})[f_{\mathrm{R}}(r_{ij}) + b_{ij} f_{\mathrm{A}}(r_{ij})] \tag{2}$$

where

$$f_{\mathrm{R}}(r_{ij}) = A_{ij} \exp(-\lambda_{ij} r_{ij}),$$
$$f_{\mathrm{A}}(r_{ij}) = -B_{ij} \exp(-\mu_{ij} r_{ij});$$
$$f_{\mathrm{C}}(r_{ij}) = \begin{cases} 1 & r_{ij} \leqslant R_{ij} \\ \frac{1}{2} + \frac{1}{2} & \\ \times \cos\left[\dfrac{\pi(r_{ij} - R_{ij})}{(S_{ij} - R_{ij})}\right], & R_{ij} \leqslant r_{ij} \leqslant S_{ij}; \\ 0 & r_{ij} \geqslant R_{ij} \end{cases}$$

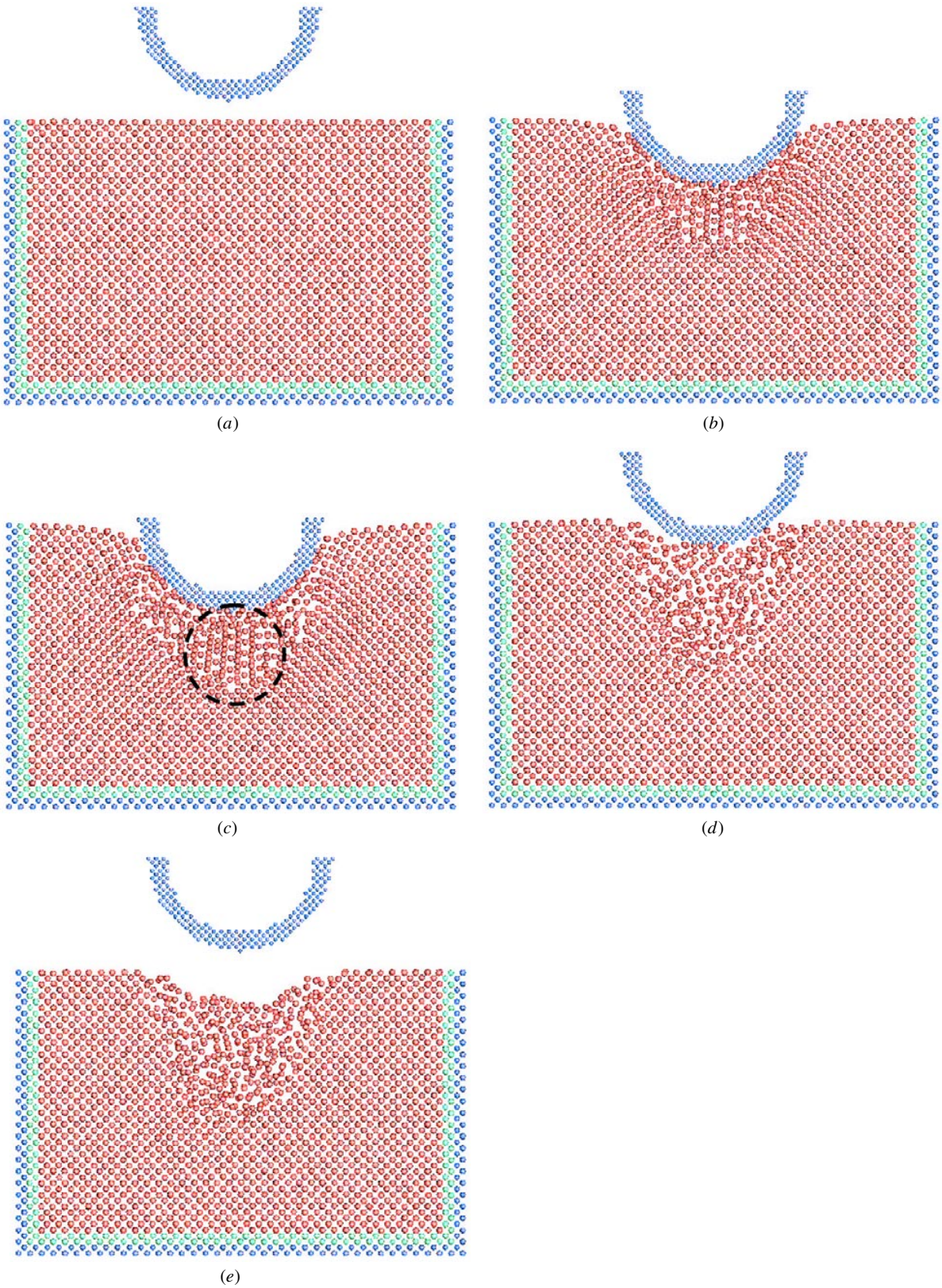

Figure 4. Positions of atoms in the silicon specimen at different stages of the indentation process. The smaller dots are diamond atoms. (*a*) Crystalline structure of diamond cubic silicon prior to indentation; (*b*) atoms beneath the indentor displaced from their original structure during indentation; (*c*) at maximum indentation, atoms beneath the indentor (circled by the dotted line) have a crystalline order different from that of the original diamond cubic structure; (*d*) long-range order of crystals is lost, leading to formation of amorphous phase during unloading; (*e*) residual amorphous phase silicon after indentation.

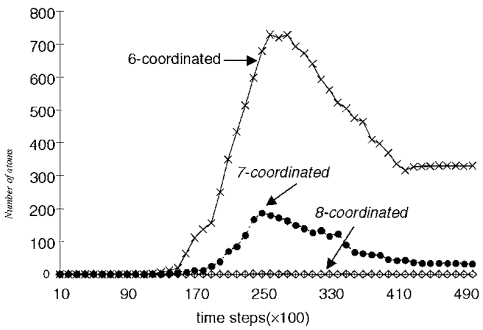

Figure 5. Graph of number of atoms with specified nearest number of neighbours against time. There is a significant increase in the number of atoms having six nearest neighbours during indentation.

Table 1. Parameters in Tersoff potential for carbon and silicon.

Parameter	Carbon	Silicon
A (eV)	1.3936×10^3	1.8308×10^3
B (eV)	3.4670×10^2	4.7118×10^2
$\lambda\mu$	34.879	24.799
μ	22.119	17.322
β	1.5724×10^{-7}	1.1000×10^{-6}
n	7.2751×10^{-1}	7.8734×10^{-1}
c	3.8049×10^4	1.0039×10^5
d	4.384×10^0	1.6217×10^1
h	-5.7058×10^{-1}	-5.9825×10^{-1}
R (nm)	0.18	0.27
S (nm)	0.21	0.30
$\chi_{c-c} = 1.0$	$\chi_{Si-Si} = 1.0$	$\chi_{C-Si} = 0.9776$

$$b_{ij} = \chi_{ij}(1 + \beta_i^{n_i}\zeta_{ij}^{n_i})^{-1/2n_i},$$

$$\zeta_{ij} = \sum_{k\neq i,j} f_C(r_{ik})g(\theta_{ijk}),$$

$$g(\theta_{ijk}) = 1 + c_i^2/d_i^2 - c_i^2/[d_i^2 + (h_i - \cos\theta_{ijk})^2];$$

$$\lambda_{ij} = (\lambda_i + \lambda_j)/2, \qquad \mu_{ij} = (\mu_i + \mu_j)/2,$$

$$A_{ij} = (A_i A_j)^{1/2}, \qquad B_{ij} = (B_i B_j)^{1/2},$$

$$R_{ij} = (R_i R_j)^{1/2}, \qquad S_{ij} = (S_i S_j)^{1/2}.$$

Other parameters such as A, B, R, S, λ, χ and μ, as listed in table 1, are Tersoff potential parameters, depending on individual materials. With equations (1) and (2), the interaction forces between silicon atoms can be obtained by calculating the gradient of E.

The interaction between the silicon atoms and the diamond indentor atoms is modelled by the Morse potential [18, 19] given by

$$\phi(r_{ij}) = \lambda_1 D[\exp\{-2\lambda_2\alpha(r_{ij} - r_0)\} - 2\exp\{\lambda_2\alpha(r_{ij} - r_0)\}].$$

The parameters such as D, α and r_0 are shown in table 2. The interaction force is calculated by the gradient of ϕ.

The choice of these potentials is supported by previous simulations and tests, which showed good agreement between simulation results and experimental data [20–22].

Table 2. Parameters in the standard Morse potential.

Parameter	C–Si
D (eV)	0.435
α (nm^{-1})	46.487
r_0 (nm)	0.194 75
λ_1	1
λ_2	1

2.3. Temperature conversion and time step for integration

The three models [23] available for conversion between the kinetic energy and temperature of an atom are the Dulong–Petit model, which takes into account the independent lattice vibration, the Einstein model, which is based on the consideration of the single characteristic frequency, and the Debye model, which involves a range of frequencies. A comparison with the experimental measurement given by Sinnott [24], see figure 3, shows that, in the temperature regime encountered in the present simulation, the Debye model is the best for silicon while the Einstein model is the most suitable for diamond. Thus these models will be used correspondingly in the atomic heat conversion in the present study.

To simulate the machining process under room-temperature conditions, the silicon atoms were arranged in a perfect diamond cubic structure with the lattice parameters equal to their equilibrium values at an ambient temperature of 23 °C. The ambient temperature is maintained by the use of the thermostat atoms that surround the control volume. During the simulation process, the temperature of the thermostat atoms is kept at 23 °C by scaling their velocities at every time step.

Another critical issue in molecular dynamics analysis is the appropriate selection of the time step for the numerical integration of the equations of motion of individual atoms. Too small a time step requires a huge computational cost but too large a time step brings about unreliable results. A suitable time step should be less than 10% of the vibration period of an atom. Hence the optimum time step is dependent on both the specific material and the potential function used.

With the Tersoff potential, an individual atom of silicon or diamond can be forced to move in a direction to show the corresponding stiffness k, so that the period of vibration of the atom in the direction T can be determined by $T = 2\pi(m/k)^{1/2}$, where m is the mass of the atom. A comparison between the molecular dynamics simulation using the Tersoff potential with experimental measurements [24] shows that a time step of 1.0 fs for diamond and 2.5 fs for silicon will provide sufficiently accurate integration.

3. Results and discussion

Snapshots of the location of the atoms of a silicon specimen at different stages during the indentation are shown in figure 4. The size of the spheres that depict silicon atoms has been deliberately reduced so that we can clearly see any changes to the crystalline order of diamond cubic silicon. At maximum

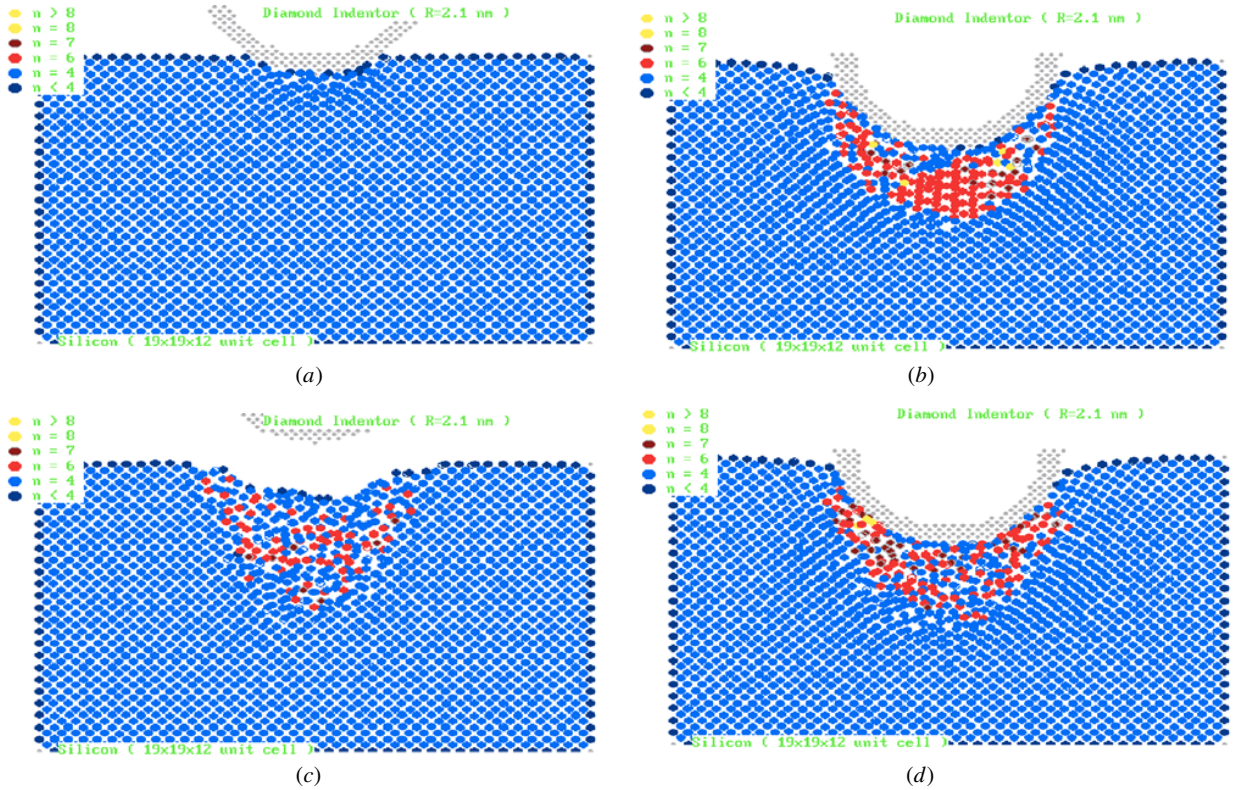

Figure 6. Number of nearest neighbours of silicon atoms at different stages of indentation: (*a*) atoms having four nearest neighbours in diamond cubic structure at the start of indentation; (*b*) atoms having six nearest neighbours predominant in the region beneath the indentor at maximum indentation; (*c*) atoms having four nearest neighbours in the amorphous state, mixed with atoms having six nearest neighbours after indentation; (*d*) atoms again predominantly having six nearest neighbours at maximum indentation during the second loading.

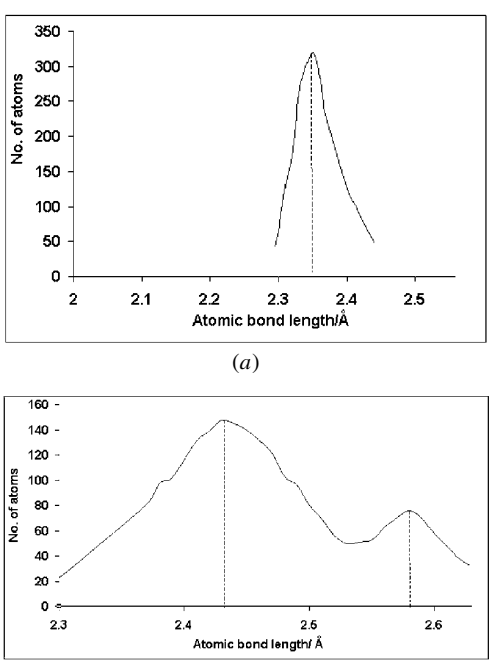

Figure 7. Length of bond at (*a*) start of indentation and (*b*) maximum indentation.

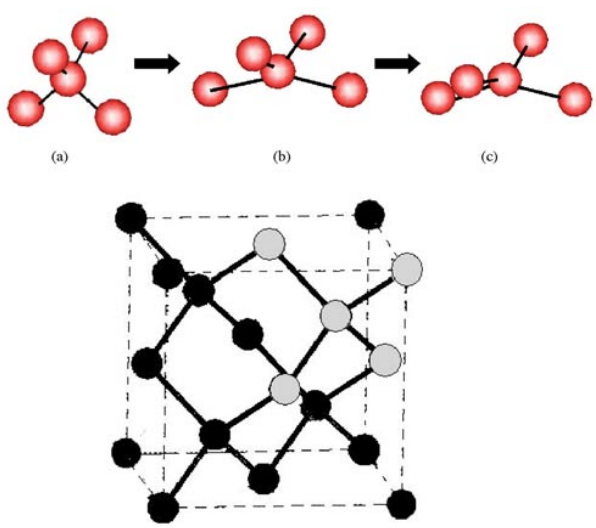

Figure 8. Flattening of the tetrahedron in the diamond cubic structure. The atoms with a lighter colour form the tetrahedron in the diamond cubic structure. The top diagram shows the change of shape of this tetrahedron during the indentation process. (*a*) Tetrahedron before indentation, (*b*) during indentation and (*c*) at maximum indentation.

indentation (figure 4(*c*)), it is observed that the order of atoms beneath the indentor differs considerably from its original pattern. However, these transformed atoms still maintain a long-range crystalline order. This suggests that a displacive phase transformation of one crystalline form of silicon to another has occurred.

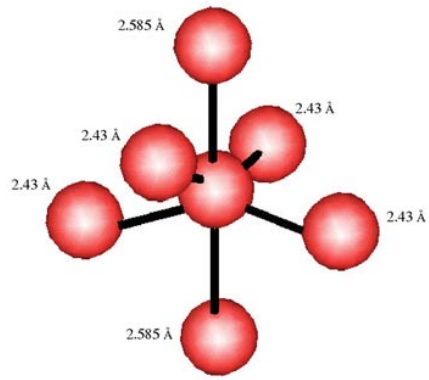

Figure 9. An atom of β-silicon with its six nearest neighbours. Four atoms are at a distance of 2.43 Å and another two at a slightly further distance of 2.585 Å.

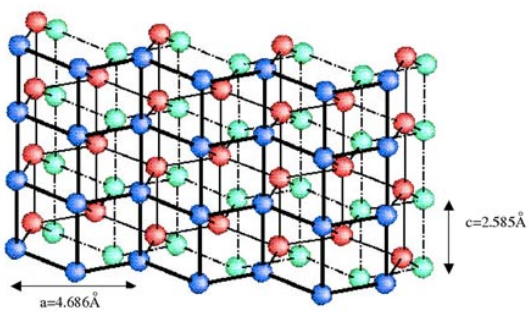

Figure 10. Crystal structure of β-silicon phase during maximum indentation.

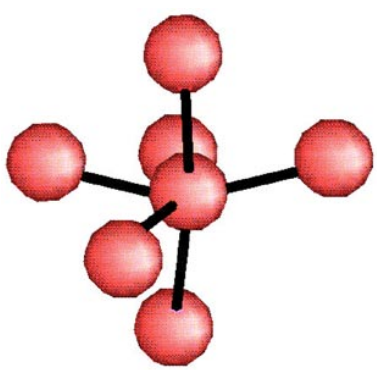

Figure 11. An atom of the distorted β-silicon obtained during the second indentation, with its six nearest neighbours.

An investigation into the coordination number of the atoms reveals that, accompanying such a transformation, there is a significant increase in the number of atoms that are six coordinated. Figure 5 shows the variation in the coordination numbers of the silicon atoms during the indentation process. This is consistent with the theoretical coordination number of an atom in the β-silicon phase. It can also be seen that the atoms that are six coordinated are formed in the region just beneath the indentor during maximum indentation. This is evident in figure 6, which shows the coordination number of each silicon atom in the specimen at different stages of the indentation. As a further investigation into the nature of the phase transformation, the bond length distributions of the atoms within the transformation zone

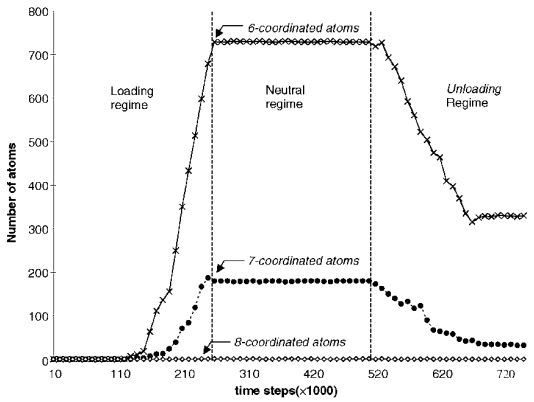

Figure 12. Number of atoms with specified nearest number of neighbours against time. In this simulation, the indentor is deliberately held at maximum indentation for 250 000 time steps, denoted as the neutral regime, to show the stability of the transformed β-silicon phase when Tersoff's potential is used.

are calculated. The results of these calculations show that during the indentation the average atomic distance between the atoms that have undergone transformation changed from 2.35 Å (diamond cubic structure) to 2.43 and 2.58 Å (β-silicon) (figure 7). From the simulation, it is found that the change is due to the flattening of the tetrahedron structure in diamond cubic silicon. The displacive transformation at progressive time steps is demonstrated in figure 8. By determining the spatial coordinates of the atoms, it is found that these four atoms of the flattened tetrahedron and another two atoms at a slightly further distance of 2.58 Å form the six nearest neighbours of the six-coordinated atoms. Figure 9 shows one of these atoms with its six nearest neighbours. At maximum indentation, about 730 atoms transform from the four-coordinated diamond cubic phase to the six-coordinated β-silicon phase. A portion of the transformed six-coordinated atoms beneath the indentor obtained from the simulation is shown in figure 10. The atoms form a repetitive crystal structure with lattice parameters $a = 4.684$ Å and $c = 2.585$ Å. These parameters of the new phase formed are in complete agreement with Donohue's description [25] of high-pressure β-silicon. The change of structure from diamond cubic to β-silicon is accomplished by displacing atoms along the c-axis with an increase in bond length and a decrease in volume. Hence the present simulation suggests that β-silicon forms beneath the indentor in the compressive stress region through displacive phase transformation during indentation.

To ensure that the β-silicon phase is not an intermediate phase obtained due to the short simulation time, the indentor's position is kept unchanged for at least 250 000 time steps at a stage with β-silicon formed (e.g. at the maximum indentation). By determining the spatial coordinates of these atoms, it is found that the β-silicon structure of atoms in the transformed zone remains unchanged in that period of time. The coordination number of the atoms is once again recorded during the simulation. Figure 12 shows the variation in the coordination number of the atoms with the number of time steps. Clearly, the number of atoms that are six-coordinated (β-silicon atoms) remains constant for the entire period when the indentor's position is held unchanged. This also indicates

that the new phase formed is not an intermediate unstable phase. However, when the indentor is unloaded, the β-silicon transforms to amorphous silicon, which will be discussed later. This means that the β-silicon phase obtained is stable as long as the required stress field is maintained.

Experimental studies [26–30] have shown that phase transformation in silicon from its normal, diamond cubic structure to the denser, β-silicon structure will take place under pure hydrostatic pressure in the range of 11–12 GPa. However, it was also found that under more complex conditions, such as in indentation, the transformation pressure may be reduced to as low as 8 GPa [7]. In the present simulation, the maximum hydrostatic pressure attained is 12 GPa, which is therefore consistent with these experimental findings. The authors are currently looking into an anisotropic stress criterion that might provide an even more accurate prediction for phase transformation in silicon.

Referring once again to figure 4, it is also observed that the crystalline order of the atoms is lost upon unloading of the indentor (figure 4(d)), and a body-centred-tetragonal-to-amorphous phase transformation has occurred. This is consistent with the observation of Clarke *et al* [28], that proposed a possible explanation for the formation of the amorphous silicon after indentation in the present study. At the relatively rapid unloading rate employed (40 m s^{-1}) and the non-hydrostatic constraint imposed on the transformed region, the high-pressure, crystalline form cannot transform back fast enough, and, without complications, the amorphous phase forms metastably.

It is interesting to note that, within this amorphous region, most of the atoms are four coordinated with the exception of some atoms that are six coordinated. This suggests that the amorphous phase consist of four-coordinated atoms but without any long-range order. The six-coordinated atoms are observed to be the crystallite remnants of the β-silicon phase, maintaining the tetragonal body-centred crystal structure, interspersed within the amorphous region. Experimental findings also lend credence to this claim [30].

In his experiments with silicon specimens subjected to hydrostatic pressure in a diamond-anvil pressure cell, Minomura [31] found that the β-silicon-to-amorphous phase transformation is in fact reversible. To examine whether this is also the case in high-speed nano-indentation, a second indentation is performed in the simulation. It is found that the β-silicon phase could indeed have recovered upon the second loading of the indentor. This conclusion is drawn from the fact that there is once again an increase in the number of six-coordinated atoms during the second indentation (figure 6(d)). However, it can be seen from figure 6(d) that the phase transformation during the second indentation is heterogeneous, with mixing of tetragonal body centred and amorphous phases. In addition to that, the β-silicon structure obtained from the indentation of amorphous silicon (the second indentation) is distorted compared to that obtained from the indentation of diamond cubic silicon during the first indentation. Figure 11 shows the six nearest neighbours of the distorted β-silicon structure. A comparison between figures 9 and 11 shows the extent of the distortion. This is also in agreement with the claims of Minomura in his experiments with silicon specimens subjected to hydrostatic pressure in a diamond-anvil pressure cell [31].

In the simulation, there is an absence of the body-centred cubic structure that is expected upon unloading of the β-silicon as observed by Hu and co-workers in their hydrostatic loading tests [32]. This may be due to the fact that the hydrostatic pressure under the indentor during loading is not high enough to affect such a transformation upon unloading. In this simulation, the maximum hydrostatic pressure under the indentor is only 12 GPa. Minomura [31] stated that, for silicon specimens subjected to pressure above 15 GPa, transformation into the body-centred cubic structure occurs on unloading. For pressure (11–15 GPa) lower than that, the β-silicon will reversibly transform into the amorphous phase as in the case for the present simulation. A theoretical investigation on this issue is currently undergoing in the authors' research laboratory.

4. Conclusions

The present study has shown that the phase transformation of silicon found experimentally in specimens loaded under hydrostatic conditions also occurs for silicon specimens under indentation at the nanometre level with a high indentation speed. The transformation involves a microstructural change from diamond cubic silicon to a tetragonal body-centred structure upon loading of the diamond indentor and a tetragonal-body-centred-to-amorphous change upon unloading of the indentor. This phase transformation could be reversible and a recovery of the tetragonal body-centred phase is observed upon a second loading of the indentor. Hence with the aid of molecular dynamics simulation, the phase transformation of diamond cubic silicon during indentation and the mechanism involved in such a transformation are clearly shown.

Acknowledgment

The authors appreciate the continuous financial support of the Australian Research Council.

References

[1] Callahan D L and Morris J C 1992 *J. Mater. Res.* **7** 1614–7
[2] Wentorf R H and Kasper J S 1963 *Science* **139** 338
[3] Bundy F J 1964 *J. Phys. Chem. Solids* **41** 3809
[4] Wittig J 1965 *Phys. Lett.* **17** 187
[5] Wittig J 1966 *Z. Phys.* **195** 215
[6] Dyuzheva T I, Kabalkina S S and Novichkov V P 1978 *Zh. Eksp. Teor. Fiz.* **74** 1784
[7] Gupta M C and Ruoff A L 1980 *J. Appl. Phys.* **51** 1072
[8] Jamieson J C 1963 *Science* **139** 762
[9] Werner A, Sanjurjo J A and Cardona M 1982 *Solid State Commun.* **44** 155
[10] Olijnyk H, Sikka S K and Holzapfel W B 1984 *Phys. Lett.* A **103**
[11] Hu J Z and Spain I L 1984 *Solid State Commun.* **51** 263
[12] Spain I L, Black D R, Merkle L D, Hu J Z and Menoni C S 1984 *High Temp.–High Pressures* **16** 507
[13] Kasper J S and Richards S M 1964 *Acta Crystallogr.* **77** 752
[14] Welber B, Kim C K, Cardona M and Rodriguez S 1975 *Solid State Commun.* **17** 1021
[15] Piermarini G J 1975 *Phys. Rev.* B **12** 1171
[16] Tersoff J 1989 *Phys. Rev.* B **39** 5566
[17] Tersoff J 1986 *Phys. Rev. Lett.* **56** 632

[18] Zhang L C, Tanaka H and Liu Z 1997 *IUTAM: Proc. 19th Int. Congr. on Theoretical Applied Mechanics (Kyoto, 1997)*
[19] Tanaka H and Zhang L C 1996 *Progress in Cutting and Grinding* ed N Narutaki *et al* (Osaka: JSPE)
[20] Zhang L C and Tanaka H 1997 Towards a deeper understanding of friction and wear on the atomic scale: a molecular dynamics analysis *Wear* **211** 44–53
[21] Zhang L C and Tanaka H 1998 Atomic scale deformation in silicon monocrystals induced by two-body and three-body contact sliding *Tribol. Int.* **31** 425
[22] Tanaka H and Zhang L C 1997 *Advances in Abrasive Technology* ed L C Zhang and N Yasunaga (Singapore: World Scientific) pp 43–7
[23] Kittel C 1996 *Introduction to Solid State Physics* 7th edn (New York: Wiley)
[24] Sinnott M J 1958 *The Solid State Physics for Engineers* (New York: Wiley) pp 291
[25] Donohue J 1974 *The Structures of the Elements* (New York: Wiley) p 262
[26] Gridneva I V, Milman Yu V and Trefilov V I 1972 *Phys. Status Solidi* a **14** 177
[27] Gerk A P and Tabor D 1978 *Nature* **271** 732
[28] Clarke D R, Kroll M C, Kirchner P D, Cook R F and Hockey B J 1988 *Phys. Rev. Lett.* **21** 2156
[29] Pharr G M, Oliver W C and Clarke D R 1989 *Scr. Metall.* **23** 1949
[30] Pharr G M, Oliver W C and Clarke D R 1990 *J. Electron. Mater.* **19** 881
[31] Minomura S 1985 *Localization and Metal–Insulator Transitions* ed H Fritzsche and D Adler (New York: Plenum) p 63
[32] Hu J Z, Merkle L D, Menoni C S and Spain I L 1986 *Phys. Rev.* B **34** 4679–84